JOURNAL OF THERMOPHYSICS AND HEAT TRANSFER
Vol. 8, No. 3, July–Sept. 1994

Numerical and Experimental Study of Three-Dimensional Liquid Sloshing Flows

Kuo-Huey Chen*
University of Toledo/NASA Lewis Research Center, Cleveland, Ohio 44135
and
Franklyn J. Kelecy† and Richard H. Pletcher‡
Iowa State University, Ames, Iowa 50011

A numerical and experimental study of three-dimensional liquid sloshing inside a partially filled spherical container is described. Solutions of the unsteady, incompressible Navier-Stokes equations are presented for two types of rotations: 1) initially-capped orbital motion, and 2) simple orbital rotation from rest to a prescribed steady-state angular velocity. The computed results from the second case are compared with experimental data from a rotating test rig fitted with two liquid-filled spherical tanks.

Introduction

THE motion of a sloshing liquid inside a moving container has long been of interest to engineers and researchers. Liquid sloshing arises in many important practical applications, including the design of oil tankers, railroad tank cars, missiles, satellites, and spacecraft.[1-5] The present study is concerned with sloshing flows inside spherical containers undergoing motions characteristic of spin-stabilized satellites. Previous research[6] in this area has shown that satellites containing partially filled fuel stores can exhibit an unstable coning motion shortly after being released in space. This instability is thought to arise from sloshing forces induced by the motion of the fuel inside the stores themselves.

One of the distinguishing characteristics of sloshing flows is the presence of one or more free surfaces. A free surface, in the present context, is defined as the interface between the liquid and another fluid (usually a gas) which fills the regions not occupied by the liquid. The free surface adds an additional difficulty to the analysis of the fluid motion since its position is usually not known a priori, and thus must be computed as part of the solution.

The motion of the liquid is governed by the three-dimensional, incompressible Navier-Stokes equations. To conveniently analyze the fluid motion, one can employ a coordinate transformation which maps a moving, noninertial coordinate system in physical space to a nonmoving coordinate system in computational space. The free surface may then be placed at one boundary of the computational domain (a practice known as "surface fitting"). Both the coordinate transformation and the desire to accommodate arbitrary motions of the container ultimately leads to the introduction of a large number of terms into the governing equations.[7] As a result, unsteady calculations based on this approach require enormous computational resources in order to obtain accurate solutions in both time and space.

The numerical model developed by the present authors[8,9] for studying complicated three-dimensional liquid sloshing flows in rotating spherical containers employs the coordinate transformation/surface fitting approach described above in conjunction with the artificial compressibility formulation for incompressible flows.[10] The resulting system of discrete equations is solved using a coupled strongly implicit (CSIP) procedure. Some previous results obtained with this model have been presented in Ref. 8. Although these results appear qualitatively correct, a rigorous assessment of their accuracy has not been made due to the lack of reliable experimental (or other numerical) data.

To date, only a few three-dimensional, transient free surface simulations using the incompressible Navier-Stokes equations have been reported in the open literature. Partom[11] discussed the numerical simulation of three-dimensional flow in a partially-filled cylinder. His work employed a three-dimensional extension of the volume of fluid (VOF) method of Hirt and Nichols.[12] Some results for several cases (both with and without the influence of gravity) were presented; however, no comparisons with experimental data were made. Sicilian and Tegart[13] described transient free surface results for free surface motion in a partially filled container during a controlled free fall. Although their predicted forces agreed with the trends in the measured data, some discrepancies still existed.

In an effort to provide validation data for the present study, use was made of an existing experimental facility which was originally developed to study the kinematics and dynamics of spin-stabilized satellites.[14] The facility consisted of a motor-driven rotating shaft on which two liquid-filled spherical tanks were mounted. The tanks were instrumented with sensors for measuring the transient free surface position at the walls of the containers. It was recognized that data obtained with these sensors could be directly compared to numerical results, thereby providing a means of validating the numerical model.

In the following sections, the mathematical formulation of the numerical model are briefly discussed, along with an overview of the numerical solution algorithm. Additional details of the formulation and algorithm are provided in Ref. 8. The experimental setup and test procedure are then described, followed by a presentation of some numerical and experimental results.

Mathematical Formulation

Governing Equations

The incompressible Navier-Stokes equations for a three-dimensional isothermal, laminar flow can be written as

$$\frac{\partial u_i}{\partial x_i} = 0 \tag{1}$$

Presented as Paper 92-0829 at the AIAA 30th Aerospace Sciences Meeting and Exhibit, Reno, NV, Jan. 6–9, 1992; received Sept. 14, 1992; revision received Nov. 23, 1993; accepted for publication Nov. 24, 1993.

*Senior Research Associate, M/S OAI. Member AIAA.
†Research Assistant, Department of Mechanical Engineering.
‡Professor, Department of Mechanical Engineering. Member AIAA.

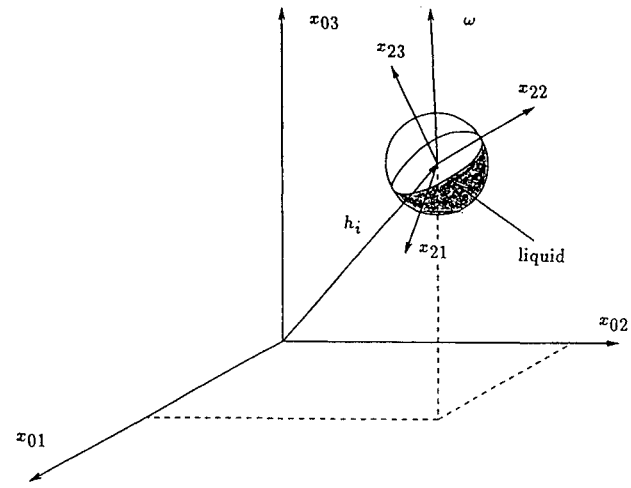

Fig. 1 Schematic of a partially filled rotating-nutating container moving relative to an inertial frame.

$$\frac{\partial u_i}{\partial t} + u_j \frac{\partial u_i}{\partial x_j} = -\frac{1}{\rho}\frac{\partial p}{\partial x_i} + \nu \frac{\partial^2 u_i}{\partial x_j \partial x_j} - g_i \tag{2}$$

where u_i are the velocity components, p is the thermodynamic pressure, g_i is the acceleration due to gravity, ρ is the density, ν is the kinematic viscosity, and x_i are the spatial coordinates ($i = 1, 2, 3$). As mentioned previously, several transformations of the governing equations are required in order to accommodate both the free surface motion and a general motion of the container with respect to an inertial coordinate system (see Fig. 1). These transformations are well documented in Refs. 7 and 8, and, therefore, will not be repeated here. Following the artificial compressibility approach of Chorin,[10] Eq. (1) is augmented with a fictitious time derivative of pressure. Upon transformation to generalized, nonorthogonal coordinates with respect to a non-inertial reference frame, the modified equations (in nondimensional form) become

$$\frac{\partial p}{\partial \tau^*} + \eta_{j,i}\frac{\partial u_{3i}}{\partial z_j} = 0 \tag{3}$$

$$\frac{\partial u_{3n}}{\partial \tau} + (\dot{z}_j + \eta_{j,i}u_{3i} + \eta_{j,i}f_{ik}x_{3k})\frac{\partial u_{3n}}{\partial z_j} - (f_{ni} + 2\lambda_{ni})u_{3i} + \eta_{j,n}\frac{\partial p}{\partial z_j} - \frac{1}{Re}\left(\eta_{j,i}\eta_{k,i}\frac{\partial^2 u_{3n}}{\partial z_j \partial z_k} + \eta_{k,ii}\frac{\partial u_{3n}}{\partial z_k}\right) = \tau_{1,ni}x_{3i} + \tau_{2,ni}h_i - g_{3n} + E_n \tag{4}$$

where u_{3i} is the relative velocity component in x_3 coordinate system (see Figs. 1 and 2), Re is the Reynolds number based on the radius of the spherical container and the rotational speed, z_j are the generalized coordinates, τ is the physical time, τ^* is the pseudotime employed in the artificial compressibility method, $\eta_{i,j}$ and $\eta_{i,jj}$ are metric terms, and $\dot{z}_i$ is the grid speed. Other quantities appearing in the above equations can be attributed to the transformation of the governing equations from an inertial to a noninertial frame. Additional details are given in Refs. 7 and 8.

Boundary Conditions

All boundary conditions are treated implicitly. Since there are four unknowns in the governing equations, four boundary equations are required to close the system. The present geometry (Fig. 2) contains only two types of boundaries: 1) the solid wall of the container, and 2) the free surface. For the solid wall, the no-slip conditions for the velocity (u, v and w) are invoked, and a boundary condition for pressure is derived by taking the dot product of the vector momentum equation

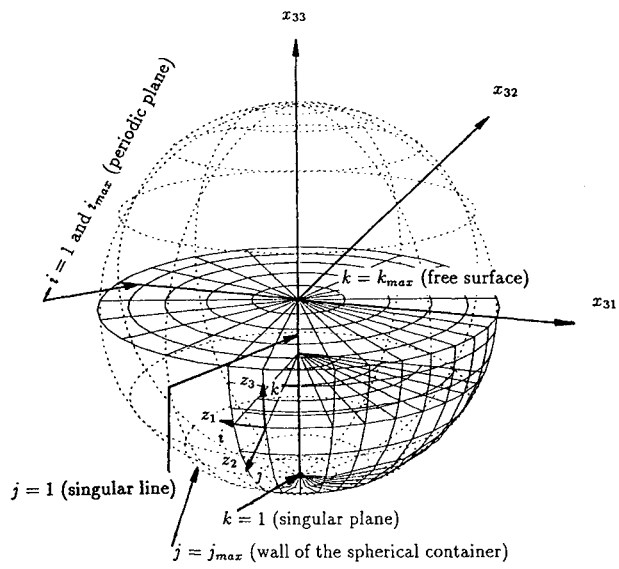

Fig. 2 Coordinate system for liquid sloshing problem.

with a unit normal at the wall. The final form of the pressure boundary condition can be found in Chen.[7]

At the free surface, four conditions are imposed to obtain the boundary equations. First, two components of the tangential shear stress along the free surface are assumed to be zero. This is justified since the external tangential forces exerted by the gas overlying the free surface are negligibly small. Second, the normal component of the shear stress is assumed to be continuous across the free surface. A further assumption is made that only the pressure contribution is significant, since the viscous stress contribution for gases is small compared with the corresponding terms for the liquid. Finally, the continuity equation, Eq. (3), must be satisfied at the free surface. Detailed expressions are provided in Chen[7] and Chen and Pletcher.[8]

The free surface position is determined by solving the kinematic equation.[15] The kinematic equation essentially represents the fact that fluid particles which initially lie on the free surface must remain on it. Letting F denote the free surface height (which is a function of the coordinates x_{31} and x_{32} and time), the kinematic equation for the free surface may be expressed as

$$(D/Dt_2)[F(x_{31}, x_{32}, t_3) - x_{33}] = 0 \tag{5}$$

This equation is used to update the free surface at each time step once the velocity field has been determined from the solution of the Navier-Stokes equations.

Numerical Solution Algorithm

Equations (3) and (4), together with the boundary conditions, yield a closed system of equations once the free surface position has been updated by the kinematic equation. A form of the artificial compressibility method (first proposed by Chorin[10]) is used to solve the equations in a coupled manner. In discretizing the equations, first-order forward differences are used for the time terms, and second-order central differences for the spatial derivatives. The metric terms have been carefully formulated in the present case so that the geometric conservation law[16] is satisfied numerically.

All nonlinear terms are linearized using the Newton linearization approach.[17] This linearization produces a coupled set of algebraic equations for the unknowns u_{3i} and p. The linearized equations can be written as

$$A^b_{i,j,k}\boldsymbol{q}_{i,j,k-1} + A^s_{i,j,k}\boldsymbol{q}_{i,j-1,k} + A^w_{i,j,k}\boldsymbol{q}_{i-1,j,k} + A^p_{i,j,k}\boldsymbol{q}_{i,j,k} + A^e_{i,j,k}\boldsymbol{q}_{i+1,j,k} + A^n_{i,j,k}\boldsymbol{q}_{i,j+1,k} + A^t_{i,j,k}\boldsymbol{q}_{i,j,k+1} = \boldsymbol{b}_{i,j,k} \tag{6}$$

or, more compactly,

$$[A]q = b \tag{7}$$

where the coefficients A^b to A^l are 4 × 4 matrices, and q is the vector of unknowns (dependent variables), $(u_{3i}, p)^T$, and b is the right-hand-side vector. The difference molecule associated with Eq. (7) can be found in Ref. 8. The resulting system of algebraic equations, Eq. (7), which includes the discretized boundary equations, was solved by the CSIP method.[7]

The solution procedure for the three-dimensional liquid sloshing calculations can now be summarized: 1) prescribe the initial conditions; 2) update the free surface position (using the kinematic equation) based on the flow solution at the previous time step; 3) generate a new computational grid under the updated free surface position; 4) construct the coefficient matrix $[A]$ and the right-hand-side vector b; 5) call the CSIP solver to update the solution (u_{3i}, p); go back to step 4 and iterate (until convergence) to create a divergence-free velocity field; and 6) go back to step 2 and move to the next time step.

Experimental Setup

A schematic of the test rig used in the orbital spin-up experiments is shown in Fig. 3. Two clear-plastic spherical containers of radius $r = 7.41$ cm were positioned a radial distance $h = 25$ cm (with respect to the center of the container) from the axis of rotation. Both containers were half-filled with liquid at room temperature. Glycerin was chosen as the test fluid for the cases discussed in this article.

The spherical containers were spun in a simple orbital motion about the axis of rotation (the drive shaft) by a dc motor connected through a series of gear boxes. The plane of this orbital motion was kept normal to the axis as shown. The rotational speed was controlled manually using a transformer, and was measured by a tachometer connected to the motor drive train.

The instrumentation for a typical spherical container is illustrated in Fig. 4. Each sphere was fitted with three light-sensitive photopotentiometers to sense the 1) inboard, 2) outboard, and 3) tangential free surface positions at the wall of the container. All three photopotentiometers were oriented normal to the equatorial plane of the sphere at the indicated circumferential positions (90 deg apart). By tinting the liquid to block light transmission, the voltage output from the photopotentiometers was made proportional to the fraction of photopotentiometer surface covered by the liquid. The sensitivity of this arrangement was enhanced by a 6-V light source located at the top of the spherical container.

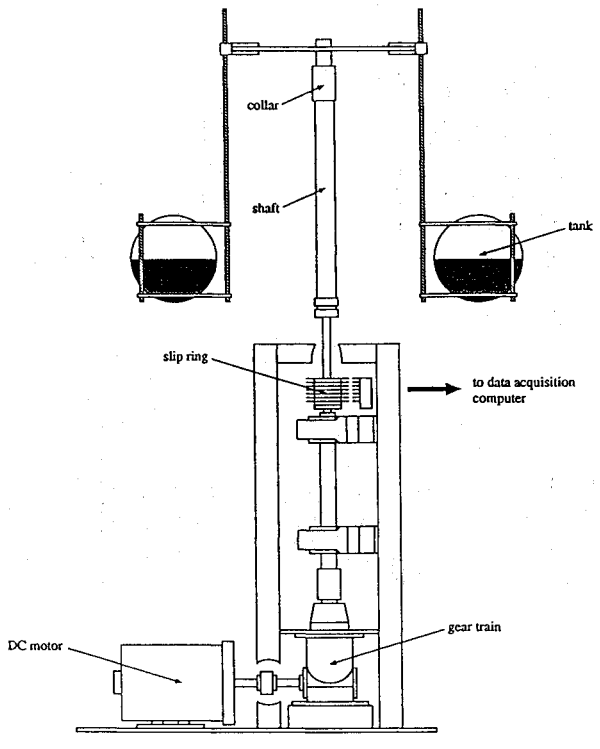

Fig. 3 Illustration of current satellite test rig configuration.

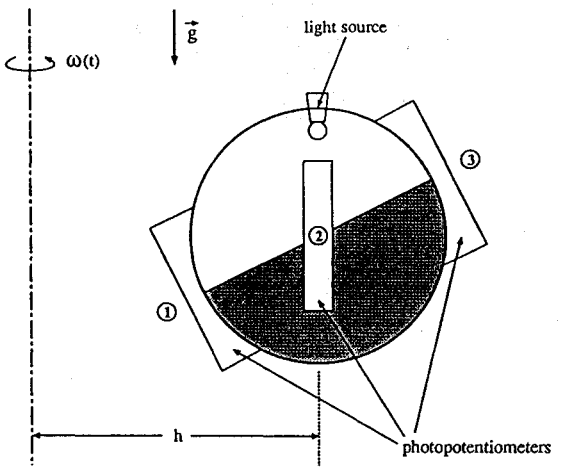

Fig. 4 Schematic of spherical container and instrumentation.

All data were collected and stored using a microcomputer outfitted with a high-speed data acquisition board. The data acquisition hardware was configured to accept eight channels of bipolar voltage signals, with a maximum sampling rate of 90,000 samples/s.

The photopotentiometers were dynamically calibrated to obtain a voltage vs free surface height relationship for use in data reduction. This calibration was accomplished by spinning the rig up to a specified rotational speed, waiting for steady-state conditions to be established, and recording the output voltage produced by the photopotentiometers. The steady-state position of the free surface (which was determined from the analytical solution for a given rotational speed) was then correlated with the known circumferential positions of the photopotentiometers.

Results and Discussion

Computations were carried out for two types of flow as described below. In both cases, terrestrial gravity was included in the acceleration field.

1) Initially-capped orbital motion: a spherical container half-filled with a liquid is spun about a specified axis of rotation at a constant rotational speed until solid-body rotation of the liquid is achieved. A cap initially covers the liquid surface to prevent it from rising up. At time zero, this cap is suddenly removed (or broken) allowing the liquid surface to rise (or drop) until another equilibrium position is reached. The initial absolute velocity is distributed according to the condition of solid-body rotation.

2) Orbital rotation from rest: a spherical container half-filled with a liquid initially at rest is gradually spun up from rest to a prescribed simple orbital motion. This case corresponds to the conditions of the experimental study.

Initially-Capped Orbital Motion

A schematic of this case is shown in Fig. 5. The radius of the container is 7.62 cm, and the distance from the axis of rotation to the center of the container is 44.7 cm. The fluid is prescribed as glycerin at room temperature.

The characteristic nondimensional parameters for this situation are

$$Re = 181.4 \qquad Fr = 3.25 \qquad We = 12002.1$$

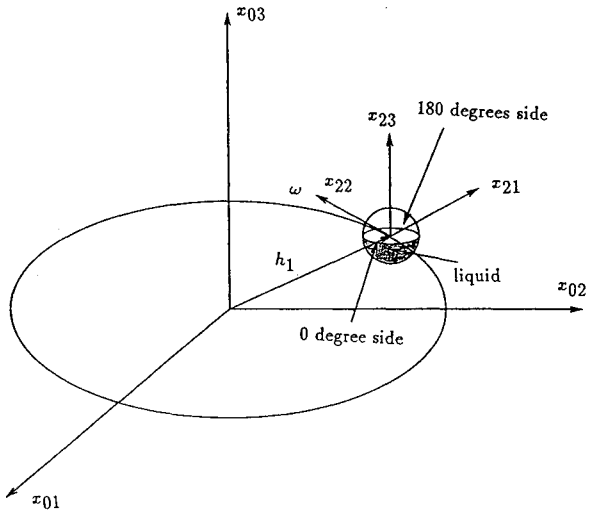

Fig. 5 Schematic for orbital rotation; container half-filled with glycerin.

where Re is the Reynolds number, Fr is the Froude number, and We is the Weber number. The Froude and Weber numbers are defined as

$$Fr = V_{\text{ref}}/\sqrt{gh}$$

$$We = \rho V_{\text{ref}} L_{\text{ref}}/\Gamma$$

where V_{ref} is the same as used in the Reynolds number, h is the initial maximum free surface depth, g is the acceleration due to gravity, and Γ is the surface tension coefficient. Since the liquid surface was covered by a cap, there was no initial free surface motion. However, it should be noted that while the initial relative velocity was zero everywhere, the absolute velocity was nonzero and distributed according to the condition of solid-body rotation.

A 51 × 11 × 11 grid (51 points in the circumferential direction), and a constant nondimensional time step of 0.01 were used for this calculation. The extremely high centrifugal force field associated with this case caused the free surface to rise (drop) almost to the top (bottom) of the tank during the transient. In addition, the motion of the free surface appeared to be more abrupt than in the cases reported in Ref. 8. This abrupt free surface motion gave rise to numerical instabilities which, in turn, resulted in a sudden divergence of the solution after a long period of time in the calculation. Upon investigating the cause of these instabilities, the following remedies were introduced into the algorithm.

First, it was found that the free surface tracking angle ϕ_r must be handled carefully (ϕ_r' is zero in this case, since there is no tangential acceleration). As described in Ref. 8, the purpose of the tracking angle is to both facilitate the present grid generation procedure and to keep the free surface height function F single-valued. The influence of the tracking angle (and its time rate of change) is contained in various terms of the transformed governing equations. For this particular case, it was observed that the free surface (and also ϕ_r) tended to oscillate after nondimensional time, $\tau = 1.8$, whereupon the time rate of ϕ_r ($\dot{\phi}_r$) began to grow rapidly. The magnitude of the terms influenced by ϕ_r in the governing equations eventually became dominant and resulted in the solution diverging. To reduce the sensitivity of the solution to this effect, the calculation of ϕ_r was modified by averaging angles at two time levels. This treatment smoothed out the temporal variations in both ϕ_r and $\dot{\phi}_r$, thereby reducing the potential for unstable behavior.

Another phenomenon observed in the present case was the appearance of a local saw-toothed profile in the free surface at a nondimensional time of $\tau = 2.6$. The propagation of this profile to neighboring points eventually resulted in a very unfavorable grid distribution, and ultimately to solution divergence. The cure for this problem was to replace the central difference approximations to the spatial derivative terms in the kinematic equation with first order upwind approximations.

The final calculations for this case were carried out on an Apollo DN10000 workstation, and required about 58 h of CPU time to reach steady state. The computed solution is presented in Figs. 6–8. A series of results showing the free

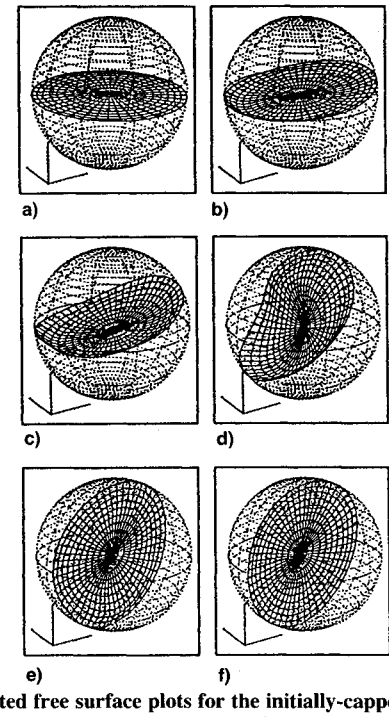

Fig. 6 Selected free surface plots for the initially-capped orbital motion of a spherical container half-filled with glycerin: τ = a) 0.0, b) 1.8, c) 2.7, d) 8.1, e) 13.5, and f) 34.2.

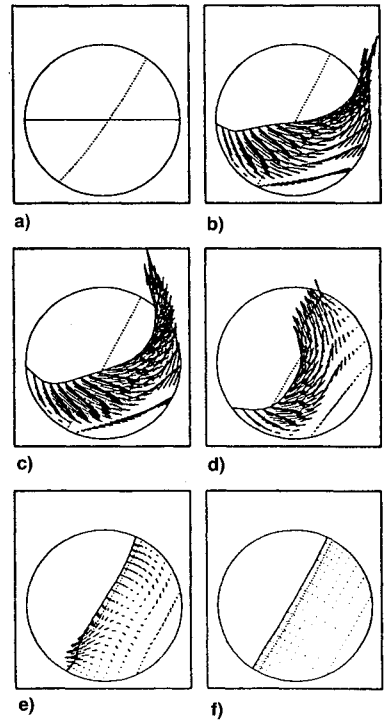

Fig. 7 Selected velocity vector plots at $x_{22} = 0$ plane for the initially-capped orbital motion of a spherical container half-filled with glycerin (The dotted line indicates the steady-state analytical free surface position): τ = a) 0.0, b) 1.8, c) 2.7, d) 8.1, e) 13.5, and f) 34.2.

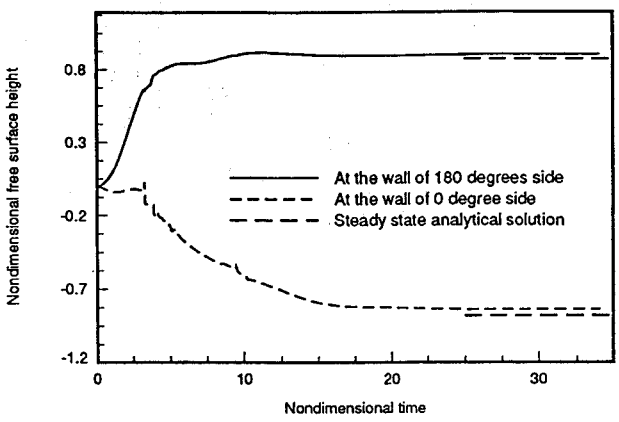

Fig. 8 Time history of the nondimensional free surface height for the initially-capped orbital motion of a spherical container half-filled with glycerin.

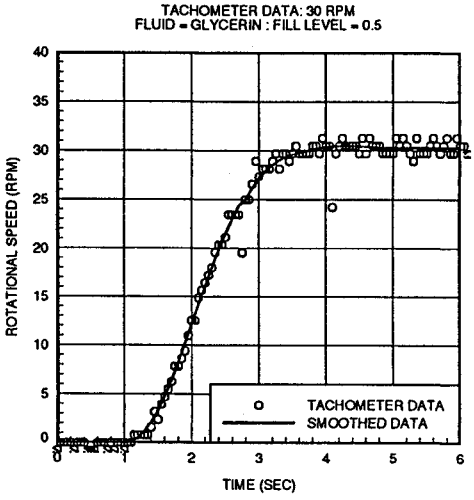

Fig. 9 Transient rotational speed curve for the orbital rotation from rest of a spherical container half-filled with glycerin: 30 rpm case.

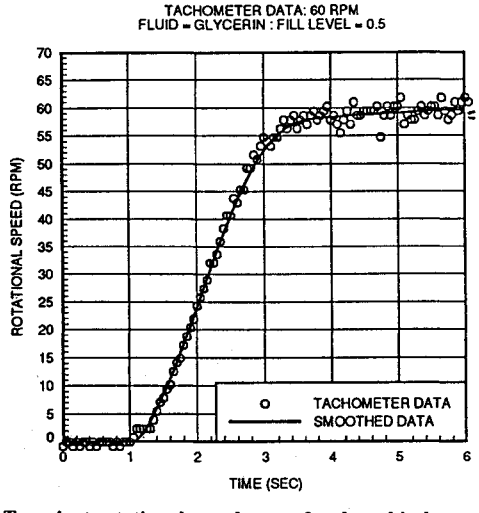

Fig. 10 Transient rotational speed curve for the orbital rotation from rest of a spherical container half-filled with glycerin: 60 rpm case.

surface position at different instants of time are shown in Fig. 6. Final steady-state conditions are achieved at about $\tau = 34$, which corresponds to approximately one revolution (orbit) of the container. The velocity vectors are presented in a similar fashion in Fig. 7.

The free surface position at the wall is shown in Fig. 8. The analytical free surface position for the steady-state, solid-body rotation condition was obtained from Ref. 7. It can be seen that some discrepancy exists between the computed steady-state free surface position and the analytical solution. It is believed that this discrepancy is either due to the use of first-order upwind differencing in the kinematic equation or to the linear interpolation procedure used to transfer the free surface points from the old grid to the new grid. Ways of eliminating these problems are currently being investigated.

Orbital Rotation from Rest

A series of experiments were carried out with the test rig to examine a gradual spin-up from rest. The variation of the rotational speed was controlled manually with the aim of producing a transient of about 1–2 s. The recorded rotational speeds (obtained from the tachometer) were then used as input to the computer program.

Due to the symmetry of the configuration, photopotentiometer data were obtained for one sphere only. During the course of calibration, it was found that the signal from the tangential photopotentiometer (no. 3) was too small to provide a reliable indication of the free surface level. This was due primarily to the small free surface deflection at that position for the tests conducted. Also, the length of the photopotentiometers (as well as other effects) limited the range of free surface deflection for which reliable calibrations of the other photopotentiometers could be obtained. Ways of extending the sensitivity and range of the photopotentiometers are currently being studied.

Two sets of data (three runs per set) were obtained for nominal steady-state speeds of 30 and 60 rpm. One run from each set was then selected for simulation with the computer program. Appropriate initial and boundary conditions were prescribed for each case, and the rotational speed as a function of time was specified using the tachometer data from the experiment. It should be noted that the tachometer data were smoothed prior to use in the program in order to filter out the noise in the signal. The resulting smoothed and unsmoothed (raw) data are shown in Figs. 9 and 10.

The numerical solutions were performed using a 41 × 11 × 11 grid (41 grid points in the circumferential direction) for 3000 nondimensional time steps ($\Delta\tau = 0.03$). Both solutions were initiated at a physical time of 1 s (the time at which the sphere begins to move in the experimental time frame). The total elapsed physical time was about 4 s. The calculations were carried out on a DECstation 5000/200, and consumed about 23 h of CPU time in both cases.

For comparison with the experiment, a nondimensional free surface height l/r was defined, where l is the height of the free surface above the equatorial plane (see Fig. 4). Values of l/r at the inboard and outboard positions were computed and stored at prescribed time intervals for later analysis. For the cases discussed below, the maximum experimental uncertainty in the values of l/r was estimated to be between 2×10^{-2} and 3×10^{-2}.

The solution for the 30-rpm case is presented in Figs. 11 and 12. In these figures, the computed inboard and outboard free surface heights are compared with their experimental counterparts. It can be seen that the computed results are in reasonable agreement with the experimental data. In particular, the delay between the initiation of the rotation and the response of the free surface appears to be well predicted, as is the general rate of change of the free surface position with time. There does, however, appear to be some smoothing of the numerical response relative to the experimental data. The differences between the numerical and experimental results are attributed to both the coarse grid used in the numerical simulation and the uncertainties inherent in the experimental data.

The solution for the 60-rpm case is presented in Figs. 13–15. For this case, the deflection of the free surface at the inboard position exceeded the calibration range, and thus could not be used. A comparison of the computed outboard free surface height response with the experimental data is shown in Fig. 13. Again, the agreement of the computations

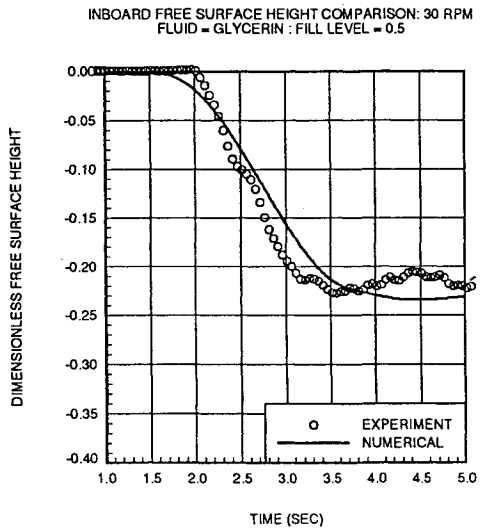

Fig. 11 Time history of the nondimensional inboard free surface height for the orbital rotation from rest of a spherical container half-filled with glycerin: 30 rpm case.

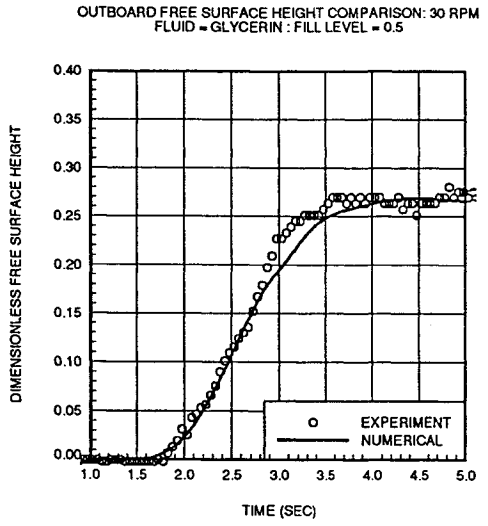

Fig. 12 Time history of the nondimensional outboard free surface height for the orbital rotation from rest of a spherical container half-filled with glycerin: 30 rpm case.

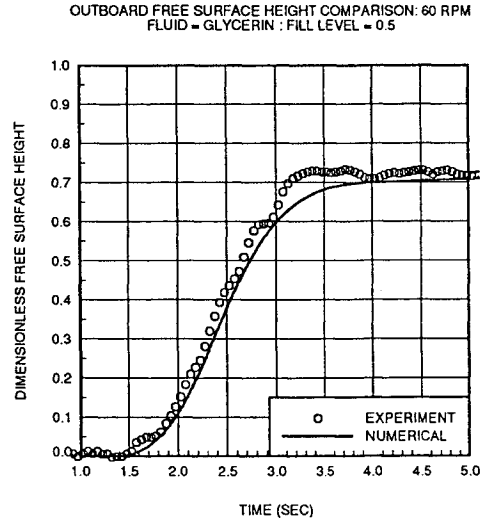

Fig. 13 Time history of the nondimensional outboard free surface height for the orbital rotation from rest of a spherical container half-filled with glycerin: 60 rpm case.

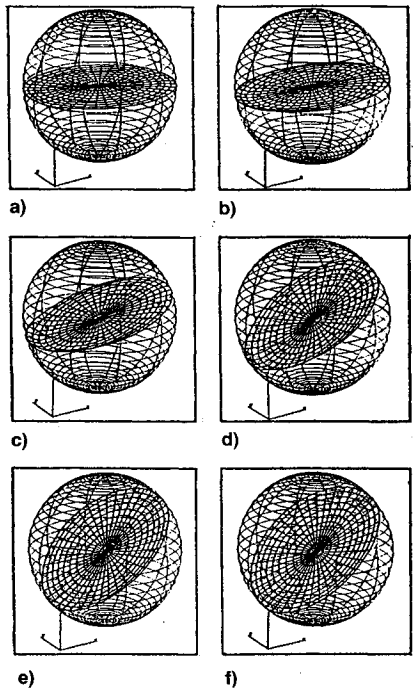

Fig. 14 Selected free surface plots for the orbital rotation from rest of a spherical container half-filled with glycerin: 60 rpm case: t = a) 1.498 s, b) 1.996 s, c) 2.494 s, d) 2.991 s, e) 3.489 s, and f) 3.989 s.

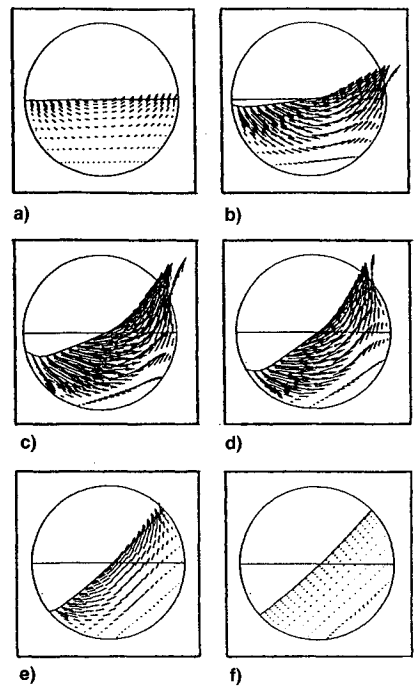

Fig. 15 Selected velocity vector plots at x_{22} = 0 plane for the orbital rotation from rest of a spherical container half-filled with glycerin: 60 rpm case (the dotted line indicates the initial free surface position): t = a) 1.498 s, b) 1.996 s, c) 2.494 s, d) 2.991 s, e) 3.489 s, and f) 3.989 s.

with experiment is generally good, although, as in the 30-rpm case, the response appears somewhat smooth.

It is observed in both cases that the free surface transient roughly corresponds to the transient in the rotational speed. This behavior is the result of the high viscosity of the test fluid (glycerin), the geometry and rotational speeds employed in the tests, and the length of the rotational speed transient. For less viscous fluids or faster transients, the motion will become more complex, with noticeable secondary oscillations persisting for some time after the steady-state rotational speed has been achieved.

Selected plots of the free surface and velocity fields are presented in Figs. 14 and 15. As the container begins to accelerate, the fluid initially sloshes both tangentially (rearward) and radially (outward), thus creating a highly distorted free surface topology. Eventually, as the steady-state conditions are approached, the free surface flattens out into its steady-state configuration.

Conclusions

Numerical solutions for two classes of three-dimensional sloshing flows inside partially filled spherical containers were presented. The calculated transient free surface positions for the orbital rotation from rest case were compared with corresponding experimental data, and found to be in reasonable agreement. Discrepancies between the numerical and experimental results were attributed to both numerical errors and experimental uncertainty. Despite these discrepancies, the essential behavior of the fluid appeared to be well predicted by the present numerical model.

Work is in progress to improve both the numerical and experimental results presented in this article. Specifically, the numerical solution procedure is being developed further so that accurate solutions can be obtained on finer grids. Improvements in the present experimental facility will include extending the accuracy and range of the photopotentiometers, and installing additional instrumentation (such as pressure transducers) at selected positions on the spherical container.

Acknowledgment

This research was supported by the Air Force Office of Scientific Research through Grant AFOSR-89-0403.

References

[1]Peterson, L. D., Crawley, E. F., and Hansman, R. J., "Nonlinear Fluid Slosh Coupled to the Dynamics of a Spacecraft," *AIAA Journal*, Vol. 27, No. 9, 1989, pp. 1230–1240.

[2]Kana, D. D., "Validated Spherical Pendulum Model for Rotary Liquid Slosh," *Journal of Spacecraft and Rockets*, Vol. 26, No. 3, 1989, pp. 188–195.

[3]Van Schoor, M. C., Peterson, L. D., and Crawley, E. F., "The Coupled Nonlinear Dynamic Characteristics of Contained Fluids in Zero Gravity," *Proceedings of the AIAA 31st Structures, Structural Dynamics, and Materials Conference*, AIAA, Washington, DC, 1990, pp. 2143–2156 (AIAA Paper 90-0996).

[4]Ramaswamy, B., "Numerical Simulation of Unsteady Viscous Free Surface Flow," *Journal of Computational Physics*, Vol. 90, No. 2, 1990, pp. 396–430.

[5]Vaughn, H. R., Oberkampf, W. L., and Wolfe, W. P., "Fluid Motion Inside a Spinning Nutating Cylinder," *Journal Fluid Mechanics*, Vol. 150, Jan. 1985, pp. 121–138.

[6]Baumgarten, J. R., Flugrad, D. R., and Prusa, J. M., "Investigation of Liquid Sloshing in Spin-Stabilized Satellites," Iowa State Univ., ISU-ERI-Ames-90401, Ames, IA, 1989.

[7]Chen, K.-H., "A Primitive Variable, Strongly Implicit Calculation Procedure for Two and Three-Dimensional Unsteady Viscous Flows: Applications to Compressible and Incompressible Flows Including Flows with Free Surfaces," Ph.D. Dissertation, Iowa State Univ., Ames, IA, Dec. 1990.

[8]Chen, K.-H., and Pletcher, R. H., "Simulation of Three-Dimensional Liquid Sloshing Flows Using a Strongly Implicit Calculation Procedure," *AIAA Journal*, Vol. 31, No. 5, 1993, pp. 901–910.

[9]Chen, K.-H., Kelecy, F. J., and Pletcher, R. H., "A Numerical and Experimental Study of Three-Dimensional Liquid Sloshing in a Rotating Spherical Container," AIAA Paper 92-0829, Jan. 1992.

[10]Chorin, A. J., "A Numerical Method for Solving Incompressible Viscous Flows Problems," *Journal of Computational Physics*, Vol. 2, No. 1, 1967, pp. 12–26.

[11]Partom, I. S., "Application of the VOF Method to the Sloshing of a Fluid in a Partially Filled Cylindrical Container," *International Journal for Numerical Methods in Fluids*, Vol. 7, No. 6, 1987, pp. 535–550.

[12]Hirt, C. W., and Nichols, B. D., "Volume of Fluid (VOF) Method for the Dynamics of Free Boundaries," *Journal of Computational Physics*, Vol. 39, No. 1, 1981, pp. 201–225.

[13]Sicilian, J. M., and Tegart, J. R., "Comparison of FLOW-3D Calculations with Very Large Amplitude Slosh Data," PVP-Vol. 176, *Computational Experiments, Proceedings of the 1989 ASME Pressure Vessels and Piping Conference* (Honolulu, HI), American Society of Mechanical Engineers, New York, 1989, pp. 23–30.

[14]Anderson, M. D., "Motion Study of a Spin Stabilized Satellite Test Rig," M.S. Thesis, Iowa State Univ., Ames, IA, 1988.

[15]Lamb, H., *Hydrodynamics*, Dover, New York, 1945.

[16]Hindman, R. G., "Generalized Coordinate Forms of Governing Fluid Equations and Associated Geometrically Induced Errors," *AIAA Journal*, Vol. 20, No. 10, 1982, pp. 1359–1367.

[17]Anderson, D. A., Tannehill, J. C., and Pletcher, R. H., *Computational Fluid Mechanics and Heat Transfer*, McGraw-Hill, New York, 1984.